

# Breakdown of half-metallic ferromagnetism in zinc-blende II-V compounds

Yun Li and Jaejun Yu\*

FPRD and Center for Theoretical Physics, Department of Physics and Astronomy, Seoul National University, Seoul 151-747, Korea

We investigated the electronic and magnetic properties of a series of zinc-blend II-V compounds by carrying out density-functional-theory calculations including spin-orbit couplings. Contrary to the case of CaN and CaP, the half-metallic characteristics of the II-V compounds such as CaSb and CaBi were found to be destroyed. Our analysis of the valence band structures of CaAs, CaSb, and CaBi revealed a critical role of the spin-orbit coupling interactions on the exchange-split band structure, thereby leading to breakdown of the half-metallic ferromagnetism for the systems with heavier group V elements in the zinc-blend II-V compounds.

PACS numbers: 71.15.Rf, 71.20.Dg, 75.50.Dd

Half-metallic ferromagnets (HMFs), being metallic in only one of the two spin channels, have been considered as an indispensable ingredient in the development of spintronic devices and applications. The realization of the half-metallicity has been investigated extensively since its first prediction on Heusler alloys by de Groot *et al.*<sup>1</sup>. However, due to the complexity in their electronic characteristics, manifesting both metallic and insulating properties in a single system at the microscopic level, HMF materials often require complex structures such as ternary spinel, Heusler, and double perovskite structures, also including transition-metal elements as a source of local magnetic moments.

To explore possible spintronics applications of HMFs to semiconductor devices, there have been a great deal of studies exploiting the half metallicity in the binary compounds of zinc-blende (ZB) structure<sup>2,3,4,5,6,7,8,9,10,11,12,13</sup>, which is simple and compatible with existing III-V and II-VI semiconductors. So far there have been a few reports on the fabrication of nano-scale MnAs dots on GaAs, CrSb ultra-thin films on the GaSb substrate, and ultra-thin CrAs layers in the CrAs/GaAs multilayers<sup>2,3,4,5</sup>. In addition, the half-metallic ZB compounds with transition-metal elements were also reported by first-principles density-functional-theory (DFT) calculations,<sup>8</sup> whereas a high Curie temperature above 400 K has been observed in experiments for CrAs and CrSb systems<sup>2,3</sup>.

Contrary to the ZB compounds containing transition-metal elements, where the localized  $d$  electrons are responsible for the ferromagnetic component in HMF, several DFT calculations have predicted another kind of ZB II-V compounds as a candidate for the HMFs *without* containing any transition-metal element<sup>10,12,13</sup>. The ZB compounds of alkaline earth elements Ca, Sr, and Ba combined with all the elements of the group V were shown to be HMFs with a magnetic moment of one Bohr magneton ( $\mu_B$ ) per formula unit-cell (f.u.). In these compounds, the presence of a flat  $p$  band crossing the Fermi level ( $E_F$ ) in its paramagnetic phase is a key to the half-metallic electronic structure. The narrow  $p$  band contributes to the exchange energy splitting close to 0.5 eV, consequently leading to an insulating gap in the majority spin channel and a metallic state in the minority spin channel.

However, since the  $p$  states of the heavy elements like Sb and Bi are affected by the relativistic spin-orbit coupling (SOC), the SOC is expected to play a role in the determination of the II-V valence band structure consisting of the an-

ion  $p$  components of As, Sb, and Bi atoms. Therefore, their ground state electronic and magnetic properties needs to be examined carefully in connection with the half-metallicity of the II-V compounds with heavy group V elements.

In this paper, we report the results of our non-collinear DFT calculations including the spin-orbit coupling terms for the electronic and magnetic properties of the ZB II-V compounds of  $AX$  ( $A$ =Ca, Sr, and Ba;  $X$ =N, P, As, Sb, and Bi). Contrary to the previous reports on the ZB II-V compounds, we found that the ZB II-V compounds containing Sb or Bi are no more half-metallic due to the strong SOC overriding the exchange instability triggered by the flat band feature of the anion  $p$  states. Our calculations showed a broad spectrum in the physical properties of the ZB II-V compounds, ranging from the half-metallic ferromagnet to an ordinary ferromagnetic metal to a paramagnetic metal. Further analysis of the valence band structures explains the competition between spin-orbit couplings and exchange interactions as a key ingredient in the determination of ground states of the ZB II-V compounds.

To investigate the role of spin-orbit coupling interactions, we carried out non-collinear DFT calculations including the SOC to determine the electronic structure and magnetic properties of the ZB II-V compounds of  $AX$  ( $A$ =Ca, Sr, and Ba;  $X$ =N, P, As, Sb, and Bi). For the self-consistent electronic structure calculations, we have optimized the equilibrium lattice constant of each  $AX$  compound under the symmetry constraint of the zinc-blende (ZB) structure. The structural stability has been extensively examined in the previous work<sup>12</sup>. It was discussed that the ZB-type structure of CaAs can exist as a metastable state under certain conditions even though neither ZB nor wurtzite (WZ) structures are the absolute ground state of CaAs. Without further discussions on the stability of the ZB structure, from now on, we like to focus on the electronic and magnetic properties of the II-V compounds at their equilibrium positions within the ZB structure.

The electronic structure calculations were performed by using the OpenMX DFT code<sup>14</sup>, a linear-combination-of-pseudoatomic-orbitals method<sup>15</sup>. The generalized gradient approximation (GGA)<sup>16</sup> was used for exchange-correlation potential. The effects of spin-orbit couplings via a relativistic  $j$ -dependent pseudopotential scheme were included in the non-collinear DFT calculations<sup>17,18,19</sup>. Double-valence-plus-single-polarization orbitals were taken as a basis set, which were generated with cutoff radii of 6.0, 6.0, and 7.0 a.u. for

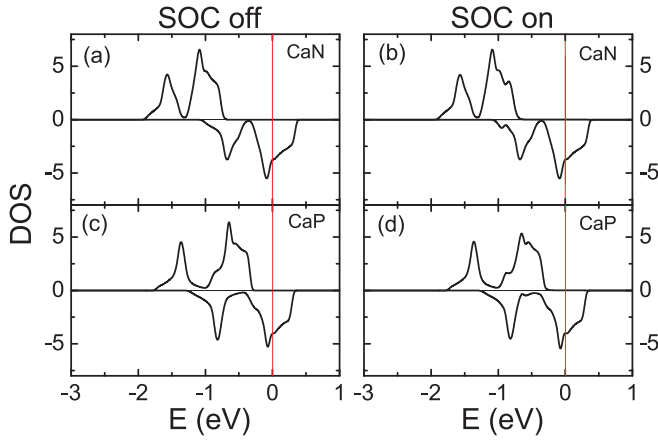


FIG. 1: Total density-of-states of CaX ( $X = N$  and  $P$ ) without and with spin-orbit coupling, as labeled by “SOC off” and “SOC on”, respectively.

Ca, Sr, Ba atoms, and 5.0, 5.5, 6.0, 6.5, and 7.0 a.u. for N, P, As, Sb, and Bi atoms, respectively. Troullier-Martins-type pseudopotentials, with a partial core correction for all atoms, were used to replace the deep core potentials by norm-conserving soft potentials in a factorized separable form with multiple projectors. The real space grid techniques were used with the energy cutoff of 300 Ry in numerical integrations and the solution of the Poisson equation using fast Fourier transformations. For the formula cell containing two atoms,  $(16 \times 16 \times 16)$   $\mathbf{k}$ -grid was sampled over the full Brillouin zone. To compare the stability of different magnetic configurations, we calculated total energies of paramagnetic (PM), ferromagnetic (FM), and anti-ferromagnetic (AFM) configurations in a supercell containing 16 atoms with  $(8 \times 8 \times 8)$   $\mathbf{k}$ -grid.

Figure 1 shows the total density-of-states (DOSs) of ZB CaN and CaP with and without spin-orbit coupling (SOC). Hereafter we denote the results with and without SOC by using the labels “SOC on” and “SOC off”, respectively. The “SOC off” and “SOC on” DOS’s for both CaN and CaP are almost identical. It is obvious that the SOC effect is negligible for the light elements like N or P atoms. Consequently the HMF character with a magnetic moment of  $1 \mu_B/\text{f.u.}$  remains unchanged regardless of the presence of SOC. In fact, the spin-orbit coupling has virtually no effect on the ZB CaN band structure, as shown in Fig. 2. While the spin-up and spin-down bands are manifest in the collinear, i.e., “SOC off” band structure of Fig. 2(a), the non-collinear band structure as obtained from the “SOC on” calculations requires a spin-resolved representation of the bands. In the spin-resolved band plots, as illustrated in Fig. 2(b) and other “SOC on” band plots in the following figures, we marked each band state by the symbols ( $\Delta$  or  $\nabla$ ), the size of which corresponds to the weight of each spin-component. Figure 2(b) clearly demonstrates that the spin-resolved band structure of CaN with negligible SOC has a clear separation of spin-up and spin-down bands, which is virtually identical to the collinear bands of Fig. 2(a).

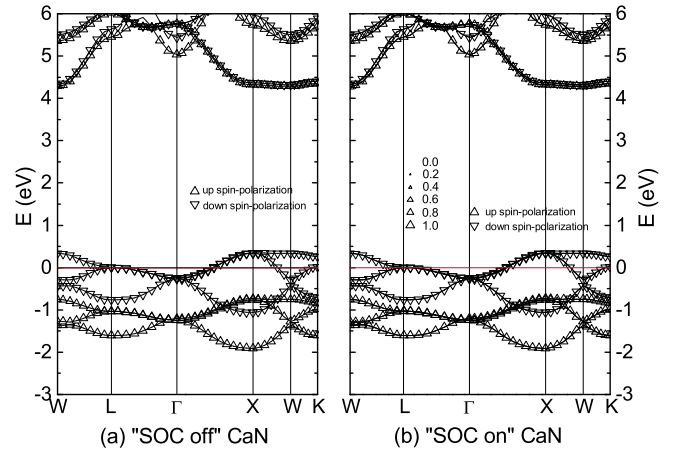


FIG. 2: Band structures of CaN (a) without (“SOC off”) and (b) with (“SOC on”) spin-orbit coupling.

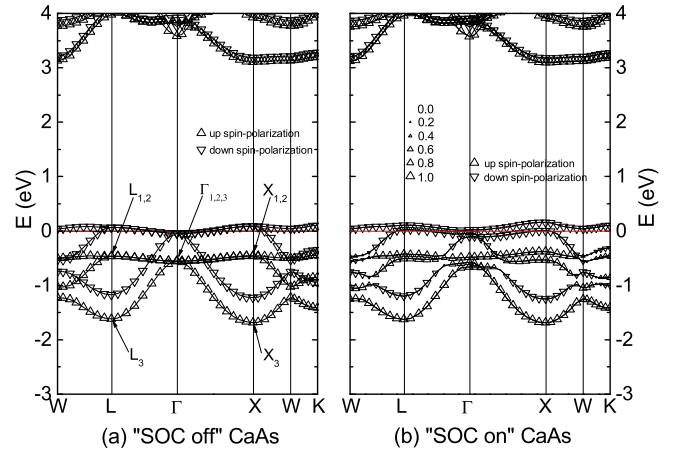


FIG. 3: “SOC off” and “SOC on” band structures of CaAs.

To demonstrate the effect of the SOC interactions on the valence band structures of the ZB II-V compounds, we have calculated the band structures of CaX ( $X = \text{As}, \text{Sb},$  and  $\text{Bi}$ ) in addition to CaN and CaP. The band plots of CaAs, CaSb, and CaBi are shown in Figs. 3, 4, and 5, respectively. One of the common features of the “SOC off” band structures of CaX is a strong exchange-splitting of the flat  $p$  bands consisting of the anion  $p$  states. The origin of magnetism for the HMF CaX compounds was attributed to the magnetic instability of the narrow  $p$  bands at the Fermi level<sup>12</sup>. In fact, the flatness of the  $p$  bands are more pronounced in the “SOC off” band structures of CaX ( $X = \text{As}, \text{Sb},$  and  $\text{Bi}$ ) than those of CaN and CaP.

The nature of the flat  $p$  bands in CaAs has been discussed in the previous work<sup>12</sup> based on the tight-binding model. We can understand the valence band structure of  $AX$  by a simple fcc lattice of anion  $X$  ( $X = \text{N}, \text{P}, \text{As}, \text{Sb},$  and  $\text{Bi}$ ) with an extraordinarily large lattice constant. In this simplified picture, for

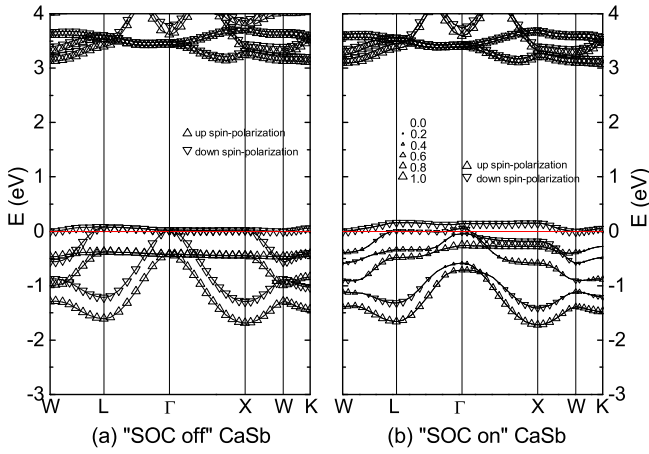


FIG. 4: “SOC off” and “SOC on” band structures of CaSb

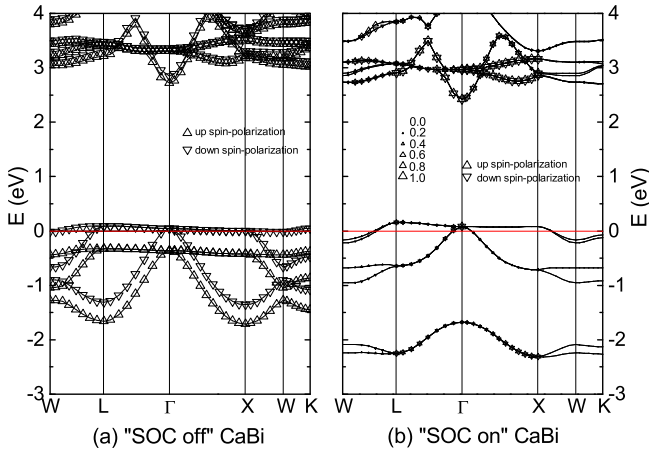


FIG. 5: “SOC off” and “SOC on” band structures of CaBi.

instance, the valence band structure of  $AX$  can be mimicked by the partially filled  $p$  bands of a fcc Br solid, which features the same  $p$  band with the same electron filling as that of  $AX$  except the flat bands observed in  $AX$ . Indeed, to acquire the flatness, the  $X$   $p$ - $p$  hybridization should be counter-balanced by the  $A$   $d$ - $X$   $p$  hybridization.

Figure 6 illustrates charge density profiles of the “SOC off” spin-up states of CaAs, which are labelled by  $\Gamma_i$ ,  $L_i$ , and  $X_i$  ( $i=1,2,3$ ) in Fig. 3(a). At the  $\Gamma$  point, the triply degenerate  $\Gamma_i$  ( $i=1,2,3$ ) states consist of  $p_x$ ,  $p_y$ , and  $p_z$  orbitals and form a anti-bonding configuration among the As  $p$  states. Due to the presence of Ca, however, the  $p$ - $p$  anti-bonding states are mixed with the Ca  $d$ -As  $p$  bonding configurations. Without the Ca  $d$ -As  $p$  bonding contribution, the energy level of the  $\Gamma_i$  states should have lied at the higher position than those shown in Fig. 3(a). As the  $k$  vector moves along  $\Gamma X$  and  $\Gamma L$ , the  $L_{1,2}$  and  $X_{1,2}$  states change into a non-bonding configuration, while the  $L_3$  and  $X_3$  states develop into a strong As  $p$ -As  $p$  bonding configuration, respectively, as illustrated in Fig. 6(c)

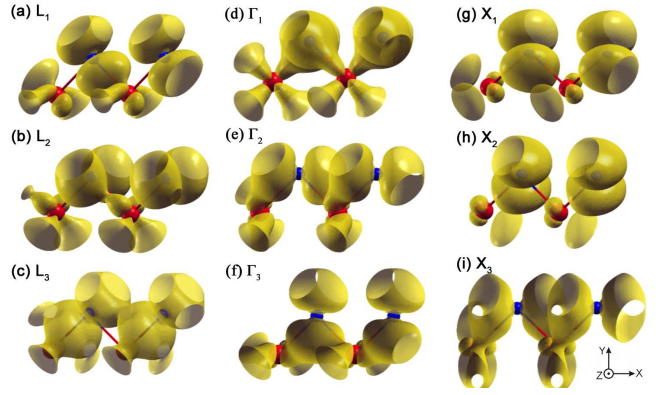


FIG. 6: (Color online) Charge density profiles of (a)  $L_1$ , (b)  $L_2$ , (c)  $L_3$ , (d)  $\Gamma_1$ , (e)  $\Gamma_2$ , (f)  $\Gamma_3$ , (g)  $X_1$ , (h)  $X_2$ , and (i)  $X_3$  states of the “SOC off” CaAs bands, which are labelled in Fig. 3(a). Light (red) spheres represent for Ca atoms and blue (dark) spheres for As atoms.

and (i). Since the nearly flat bands of the doubly degenerate  $L_{1,2} - \Gamma_{1,2} - X_{1,2}$  states contribute to the high DOS at  $E_F$ , when the SOC is turned off, the Stoner instability would drive the system into the ferromagnetic ground state.

Now let us consider the effect of spin-orbit coupling interactions on the valence band structure. When SOC is turned on, contrary to the robust HMF band structures of CaN and CaP, the electronic structures of CaX ( $X=As, Sb, \text{ and } Bi$ ) change remarkably. Despite that the “SOC off” valence bands of all the CaX ( $X=As, Sb, \text{ and } Bi$ ) compounds are almost identical as shown in Fig. 3–5, the band dispersion and spin characters of the “SOC on” band structures are markedly different and evolve as the atomic number of the element  $X$  increases from As to Sb to Bi. Since the SOC strength becomes larger for the heavier atoms, the spin-resolved band structures exhibit more complicated features. Before discussing the details of the SOC effects on the spin-resolved band structures, let us examine the evolution of the “SOC on” DOS of CaX ( $X=As, Sb, \text{ and } Bi$ ).

The “SOC off” DOSs of CaX ( $X=As, Sb, \text{ and } Bi$ ) in Fig. 7(a), (c) and (e) have basically the same characteristics as those of CaN and CaP in Fig. 1(a) and (c) except the pronounced flatness in the CaX DOSs. As the SOC strength increases from CaAs to CaSb, the sharp peaks corresponding to the flat  $p$  bands broaden and the spin-up and down components seem to smear into each other. (See Fig. 7(d) of CaSb.) For the CaBi case, where the SOC energy scale is dominant, the DOS feature shows no spin-polarization but a clear separation of two peaks: one centered at  $-2.2$  eV corresponding to the  $j=1/2$  state and the other at  $-0.5$  eV to  $j=3/2$ , as shown in Fig. 7(f) of CaBi.

In addition to the evolution of the DOS features, one can observe the change of spin-polarization (SP) at  $E_F$  as well as the magnetic moment ( $M$ ). The change of SP can be easily understood from the “SOC on” DOS plots of Fig. 7. The spin-polarization of CaAs is close to but not exactly 100%, which means that CaAs is not a HMF in a strict sense, whereas the spin-polarization of CaBi is zero. While the half-metallicity

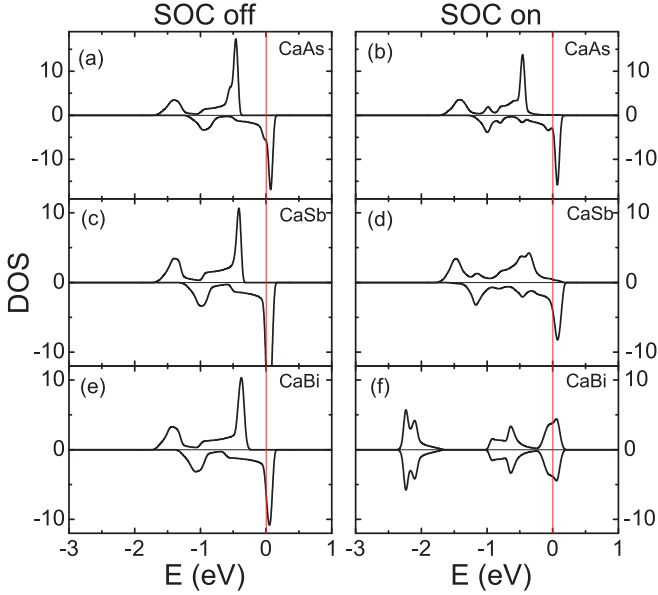


FIG. 7: Total density-of-states of  $\text{CaX}$  ( $X=\text{As, Sb, and Bi}$ ) without (“SOC off”) and with (“SOC on”) spin-orbital coupling.

TABLE I: Spin-polarization (SP) at Fermi level and magnetic moment ( $M$ )  $\mu_B/\text{f.u.}$  as obtained from the “SOC on” calculations.

	N	P	As	Sb	Bi
	SP / $M$	SP / $M$	SP / $M$	SP / $M$	SP / $M$
Ca	1.00 / 1.00	1.00 / 1.00	0.96 / 1.10	0.81 / 1.11	0 / 0
Sr	1.00 / 1.00	1.00 / 1.00	0.97 / 1.10	0.84 / 1.17	0 / 0
Ba	1.00 / 1.00	1.00 / 1.00	0.97 / 1.03	0.79 / 1.00	0 / 0

in CaAs and CaSb is destroyed moderately, the half-metallic character of CaBi disappears completely.

Table I summarizes the spin polarization (SP) at  $E_F$  and the magnetic moment ( $M$ ) of  $\text{AX}$  ( $A=\text{Ca, Sr, and Ba; } X=\text{N, P, As, Sb, and Bi}$ ). Here the SP is defined by the ratio of the spin-up and spin-down DOS at  $E_F$  over the total DOS at  $E_F$ . The magnetic moments in Table I include the contribution from both the spin and orbital moments as obtained from the non-collinear calculations. Due to the smearing of the spin-up and down components near  $E_F$ , both As and Sb compounds have non-negligible contribution of the majority spin DOS at  $E_F$ . The mixed spin-components in the valence bands are clearly shown in the spin-resolved band structures of Fig. 3(b) and Fig. 4(b). As the SOC strength increases, some of the non-collinear band states have a strong mixture of spin-up and down components.

The “SOC on” band structures of  $\text{CaX}$  ( $X=\text{N, P, As, Sb, and Bi}$ ) shown in Fig. 2–5 can be classified into three categories: (i) the CaN-type where the spin-exchange energy of  $\Delta E_{ex} \approx 0.5$  eV is dominant, (ii) the CaBi-type where  $j=1/2$  and  $j=3/2$  bands are well separated by the SOC energy scale of  $\Delta E_{so} \approx 2$  eV, and (iii) the CaSb-type, an intermediate case where both  $\Delta E_{ex}$  and  $\Delta E_{so}$  compete with each other. In the

TABLE II: Exchange and spin-orbit splitting energies in  $\text{AX}$  ( $A=\text{Ca, Sr, and Ba; } X=\text{As, Sb, and Bi}$ ). Energies are in eV unit.

	As	Sb	Bi
	$\Delta E_{ex} / \Delta E_{so}$	$\Delta E_{ex} / \Delta E_{so}$	$\Delta E_{ex} / \Delta E_{so}$
Ca	0.51 / 0.25	0.44 / 0.52	0.41 / 1.88
Sr	0.51 / 0.23	0.44 / 0.52	0.41 / 1.77
Ba	0.48 / 0.21	0.41 / 0.47	0.43 / 1.62

case of (i) the CaN-type, the SOC interactions are negligible, i.e.,  $\Delta E_{ex} \gg \Delta E_{so}$ , so that the ferromagnetic band structure is set by the exchange instability triggered by the narrow  $p$  bands. On the other hands, to understand the band structures of the types (ii) and (iii), one has to consider both SOC and exchange interactions on the same basis. To estimate the magnitudes of  $\Delta E_{ex}$  and  $\Delta E_{so}$ , we calculated the exchange and spin-orbit splitting energies at the  $\Gamma$ -point for the “SOC off” ferromagnetic and “SOC on” paramagnetic states, respectively. The calculated values of  $\Delta E_{ex}$  and  $\Delta E_{so}$  for  $\text{AX}$  ( $A=\text{Ca, Sr, and Ba; } X=\text{As, Sb, and Bi}$ ) are listed in Table II.

For the case of (ii) the CaBi-type, the SOC energy of  $\Delta E_{so} = 1.88$  eV is much larger than the effective exchange energy of  $\Delta E_{ex} = 0.41$  eV. Since the SOC term dominates, the valence band eigenstates of CaBi at the  $\Gamma$ -point are well represented by  $j=3/2$  and  $j=1/2$  states, corresponding to the 4-fold and 2-fold degeneracy, respectively. Even away from the  $\Gamma$ -point, the spin-up and down components are mixed up by maintaining its character of the spin-orbit coupled  $j$ -states. Consequently the average spin-polarization in CaBi becomes null so that the ground state is non-magnetic.

The valence band structures of CaSb, SrSb, and BaSb are much more complicated as the energy scales of the SOC and exchange interactions become comparable to each other. For an example, as listed in Table II, the SOC and exchange energies for CaSb are  $\Delta E_{so} = 0.52$  eV and  $\Delta E_{ex} = 0.44$  eV, respectively. The overall shape of the “SOC on” valence bands of CaSb in Fig. 4(b) resembles those of the “SOC off” valence bands in Fig. 4(a), whereas the degeneracy of the bands along  $L-\Gamma-X$  is significantly destroyed. Due to the strong contribution of  $\Delta E_{so}$ , the spin-flip term ( $L_+S_- + L_-S_+$ ) in the SOC term of  $\mathcal{H}_{so} = \lambda_{so}\mathbf{L} \cdot \mathbf{S}$  acts as a perturbation to the exchange-split states.

In conclusion, we have shown that the half-metallic ferromagnetism in ZB II-V compounds can be destroyed for  $\text{AX}$  ( $A=\text{Ca, Sr, and Ba; } X=\text{As, Sb, and Bi}$ ) due to the presence of strong spin-orbit coupling interactions. Our non-collinear DFT calculations revealed the evolving features of the spin-orbit coupling and exchange-split in the spin-resolved band structures as the atomic number increases from As to Sb to Bi. Considering the variation of the spin polarizations of ZB II-V compounds, it is suggested that one can control the SOC strength to design either HMF or paramagnetic metal. This SOC-dependent feature may be useful in the spintronics application of HMF materials.

We are grateful to Prof. J. I. Lee for helpful suggestions and discussions. This work was supported by the KRF Grant (MOEHRD KRF-2005-070-C00041). We also acknowledge

the support from KISTI (Korea Institute of Science and Technology Information) under The Supercomputing Application

Focus Support Program.

- 
- \* Corresponding author. Electronic address: [jyu@snu.ac.kr](mailto:jyu@snu.ac.kr)
- <sup>1</sup> R.A. de Groot, F.M. Mueller, P.G. van Engen, and K.H.J. Buschow, *Phys. Rev. Lett.* **50**, 2024 (1983).
  - <sup>2</sup> J.H. Zhao, F. Matsukura, K. Takamura, E. Abe, D. Chiba, and H. Ohno, *Appl. Phys. Lett.* **79**, 2776 (2001).
  - <sup>3</sup> H. Akinaga, T. Manago, and M. Shirai, *Jpn. J. Appl. Phys.* **39**, L1118 (2000).
  - <sup>4</sup> M. Mizuguchi, H. Akinaga, T. Manago, K. Ono, M. Oshima, M. Shirai, M. Yuri, H.J. Lin, H.H. Hsieh, and C.T. Chen, *J. Appl. Phys.* **91**, 7917 (2002).
  - <sup>5</sup> K. Ono, J. Okabayashi, M. Mizuguchi, M. Oshima, A. Fujimori, and H. Akinaga, *J. Appl. Phys.* **91**, 8088 (2002).
  - <sup>6</sup> Y.Q. Xu, B.G. Liu, and D.G. Pettifor, *Phys. Rev. B* **66**, 184435 (2002).
  - <sup>7</sup> W.H. Xie, and Y.Q. Xu, B.G. Liu, and D.G. Pettifor, *Phys. Rev. Lett.* **91**, 037204 (2003).
  - <sup>8</sup> I. Galanakis and P. Mavropoulos, *Phys. Rev. B* **67**, 104417 (2003).
  - <sup>9</sup> B. Sanyal, L. Bergqvist, and O. Eriksson, *Phys. Rev. B* **68**, 054417 (2003).
  - <sup>10</sup> K. Kusakabe, M. Geshi, H. Tsukamoto, and N. Suzuki, *J. Phys.:Condens. Matter* **16**, S5639 (2004).
  - <sup>11</sup> K. L. Yao, G. Y. Gao, Z. L. Liu, and L. Zhu, *Solid State Commun.* **133**, 301 (2005).
  - <sup>12</sup> M. Sieberer, J. Redinger, S. Khmelevskiy, and P. Mohn, *Phys. Rev. B* **73**, 024404 (2006).
  - <sup>13</sup> K. L. Yao, J. L. Jiang, Z. L. Liu, and G. Y. Gao, *Phys. Lett. A* **359**, 326 (2006).
  - <sup>14</sup> The OpenMX DFT code is available at the web site (<http://www.openmx-square.org/>) in the constitution of the GNU General Public Licence.
  - <sup>15</sup> T. Ozaki, *Phys. Rev. B* **67**, 155108 (2003); T. Ozaki and H. Kino, *Phys. Rev. B* **69**, 195113 (2004).
  - <sup>16</sup> J.P. Perdew and K. Burke, and M. Ernzerhof, *Phys. Rev. Lett.* **77**, 3865 (1996).
  - <sup>17</sup> A. H. MacDonald and S. H. Vosko, *J. Phys. C: Solid State Phys.* **12**, 2977 (1979).
  - <sup>18</sup> G. B. Bachelet, D. R. Hamann, and M. Schluter, *Phys. Rev. B* **26**, 4199 (1982).
  - <sup>19</sup> G. Theurich and N. A. Hill, *Phys. Rev. B* **64**, 073106 (2001).